3D PRINTING AND ADDITIVE MANUFACTURING
Volume 10, Number 2, 2023

DOI: 10.1089/3dp.2021.0072

ORIGINAL ARTICLE

Printing Parameters of Fused Filament Fabrication Affect Key Properties of Four-Dimensional Printed Shape-Memory Polymers

Katy Pieri,[1–3] Bailey M. Felix,[1–3] Teng Zhang,[2–4] Pranav Soman,[1–3] and James H. Henderson[1–3]

Abstract

Extrusion-based (fused filament fabrication) three-dimensional (3D) printing of shape-memory polymers (SMPs) has the potential to rapidly produce highly customized smart-material parts. Yet, the effects of printing parameters on the shape-memory properties of printed SMPs remain poorly understood. To study the extent to which the 3D printing process affects the shape-memory properties of a printed SMP part, here temperature, extrusion rate multiplier, and fiber orientation were systematically varied, and their effect on shape-memory fixing and recovery ratios was evaluated. Fiber orientation, as determined by print path relative to the direction(s) of loading during shape-memory programming, was found to significantly impact the fixing ratio and the recovery ratio. Temperature and multiplier had little effect on either fixing ratio or recovery ratio. To facilitate the use of printed SMP parts in biomedical applications, a cell viability assay was performed on 3D-printed samples prepared using varied temperature and multiplier. Reduction in multiplier was found to increase cell viability. The results indicate that fiber orientation can critically impact the shape-memory functionality of 3D-printed SMP parts, and that multiplier can affect cytocompatibility of those parts. Thus, researchers and manufacturers employing SMPs in 3D-printed parts and devices could achieve improved part functionality if print paths are designed to align fiber direction with the axis(es) in which strain will be programmed and recovered and if the multiplier is optimized in biomedical applications in which a part will contact cells.

Keywords: shape fixing ratio, shape recovery ratio, SMP MM-4520, thermoplastic polyurethane elastomer

Introduction and Background

Introduction

As the popularity of employing shape-memory polymers (SMPs) for basic science[1–5] and biomedical applications[6–9] grows, and as three-dimensional (3D) printing of SMPs grows simultaneously,[10–12] the ability to precisely control the shape-memory behavior of a printed SMP part is crucial. For example, the potential exists for implementing SMPs in applications such as minimally invasive surgery, where laparoscopes place small SMP devices, which are then expanded to a larger, permanent form once positioned.[13] However, printing parameters during fabrication could render a device ineffective or even dangerous to patients if a 3D-printed cardiovascular stent[14] was to only partially, or not reliably, recover—thereby not opening the vessel. The inability to hold a temporary shape would be equally detrimental, as the stent could start expanding in the body before reaching the deployment site. 3D-printed SMP bone anchor device would have similar challenges, where poor fixing and unreliable recovery would prevent a proper fit.[15]

Here, our goal was to determine the effect of the printing process on shape-memory behavior. To achieve this, three

[1]Syracuse Biomaterials Innovation Facility, Syracuse University, Syracuse, New York, USA.
[2]BioInspired Syracuse: Institute for Material and Living Systems, Syracuse University, Syracuse, New York, USA.
Departments of [3]Biomedical and Chemical Engineering, and [4]Mechanical and Aerospace Engineering, Syracuse University, Syracuse, New York, USA.

critical and commonly controlled printing parameters—temperature, extrusion rate multiplier, and fiber orientation—were systematically varied when printing dogbone samples. The effect of the parameters on shape-memory behavior was quantified by measuring shape fixing and recovery. In addition, because the commercially available SMP used in the work is designed for biomedical application, a viability assay was carried out to determine the extent to which printing parameters affect the SMP's previously established cytocompatibility.[16–18]

Background

Fused filament fabrication (FFF) is a widely used method of additive manufacturing that enables 3D printing of complex parts using a continuous thermoplastic filament. The filament is heated to its melting temperature and deposited in layers to print the part from the bottom-up. The print path is created using slicing software from computer-aided design (CAD) drawings, which, in combination with the deposition process, results in an efficient and low-cost method for building complex part architectures.[19] The accessibility of FFF technology for both researchers and consumers has enabled 3D printing to be used not only as a method of rapid prototyping but also as a method of primary fabrication of new parts.

FFF is one of several methods that have been employed in the development of four-dimensional (4D) printing—the 3D printing of smart materials—wherein the dynamic, time-dependent functionality of the smart material provides the ''fourth'' dimension.[20,21] 4D printing produces structures with the capacity to change form or function when triggered by an external stimulus.[22] The stimulus can be physical (such as heat[13,23]), electrical,[24,25] or even biochemical.[26] Structures produced through 3D printing can be complex and highly tailorable, making 4D printing a useful fabrication option for parts made from smart materials. FFF was chosen for this study because it is arguably more widely used and easily democratized than other 3D printing technologies (e.g., Polyjet, Digital Light Processing).[27]

SMPs are materials of growing interest for many 4D printing applications. SMPs offer relatively low processing temperatures and costs, when compared with shape-memory alloys, and the capacity for shape-changing functionality, when compared with composites. SMPs are a class of smart material with the ability to remember an original shape, be deformed and fixed into a temporary shape, and later return to the original shape when triggered by an external stimulus. To fix (program) an SMP, the polymer is first heated above its transition temperature (T_{trans}), for example glass transition temperature (T_g) or melting temperature (T_m), and configured into a new, temporary shape. The polymer is then cooled back below T_{trans} to immobilize the polymer chains and store the strain energy within the geometry through vitrification or crystallization. To return the SMP back to the original shape, an external triggering stimulus (e.g., heat[13,23,28–30]) is applied, which remobilizes the polymer chains and releases the strain.

Two metrics of the shape-memory effect that are critical to the understanding of the functionality of SMP structures are the shape fixing and shape recovery ratios. The fixing ratio characterizes the ability of an SMP to hold its temporary shape. The recovery ratio characterizes the ability of an SMP to return to its original, permanent shape.

Although several studies have examined the extent to which the parameters of the 3D printing process affect physical properties[31–33] and quality[32,34] of printed SMP parts, fundamental questions as to the effect of 3D printing on shape-memory behavior remain. Villacres *et al.* found that printing angle and infill percentage significantly impact SMP ultimate tensile stress, elastic modulus, and maximum strain.[31] Yang *et al.* studied the effect of processing parameters on SMP part density, dimensional accuracy, and surface roughness.[32] Abuzaid *et al.* studied the relationship between fiber orientation and shape change to understand part shrinkage.[34] Garcia Rosales *et al.* looked at the effect of print speed, layer height, and print temperature on Young's modulus, fixing ratio, and recovery ratio.[33] While that study found that higher temperatures, higher layer heights, and lower speeds led to higher Young's modulus, the findings for fixing and recovery ratios were only reported for samples printed using a single set of parameters (temperature, speed, and layer height of 235°C, 100 mm/s, and 0.25 mm, respectively) and were affected by the amount of strain programmed into the sample during testing, providing preliminary evidence that printing parameters affect fixing and recovery but not exploring the relationship between the printing parameters and the shape fixing and recovery ratios.

Thus, prior investigations have established that printing speeds and temperatures can affect physical properties and part quality, yet the extent to which the 3D printing process affects shape-memory behavior, including shape fixing and recovery, remains underexamined and poorly understood. Until such understanding is achieved, accurate design, precise high-fidelity printing, and reproducible shape-memory actuation of 3D-printed SMP parts are unlikely to be realized.

Methods

To investigate the extent to which printing parameters affect fixing, recovery, and cytocompatibility, dogbone samples and cell-culture substrates were produced using systematically varied nozzle temperature, extrusion multiplier, and fiber orientation (Fig. 1). Fixing and recovery ratios for each sample were calculated after conducting a one-way shape-memory cycle (1WSMC) using a dynamic mechanical analyzer (DMA). To study cytocompatibility, cells were seeded onto printed substrates and viability assessed using a LIVE/DEAD assay. Complete methodology for the following method sections can be found in Supplementary Data.

Sample preparation

A commercially available semicrystalline thermoplastic polyurethane (MM-4520; SMP Technologies, Inc., Japan) packaged as pellets was used for all experiments. This SMP was chosen because of its demonstrated success with fused filament 3D printers[32,33,35] and cytocompatibility.[16–18]

Raster-printed samples. Dogbones were designed by CAD (Autodesk Inventor, Autodesk, USA, 2019) to comply with the ASTM dogbone type IV standard, scaled down by a factor of 4. Temperature, extrusion rate multiplier, and fiber orientation were varied for each sample set. Nozzle temperature is the temperature at which the heating element located in the printer's extruder is set during printing. Extrusion multiplier controls the volume of polymer extrusion relative

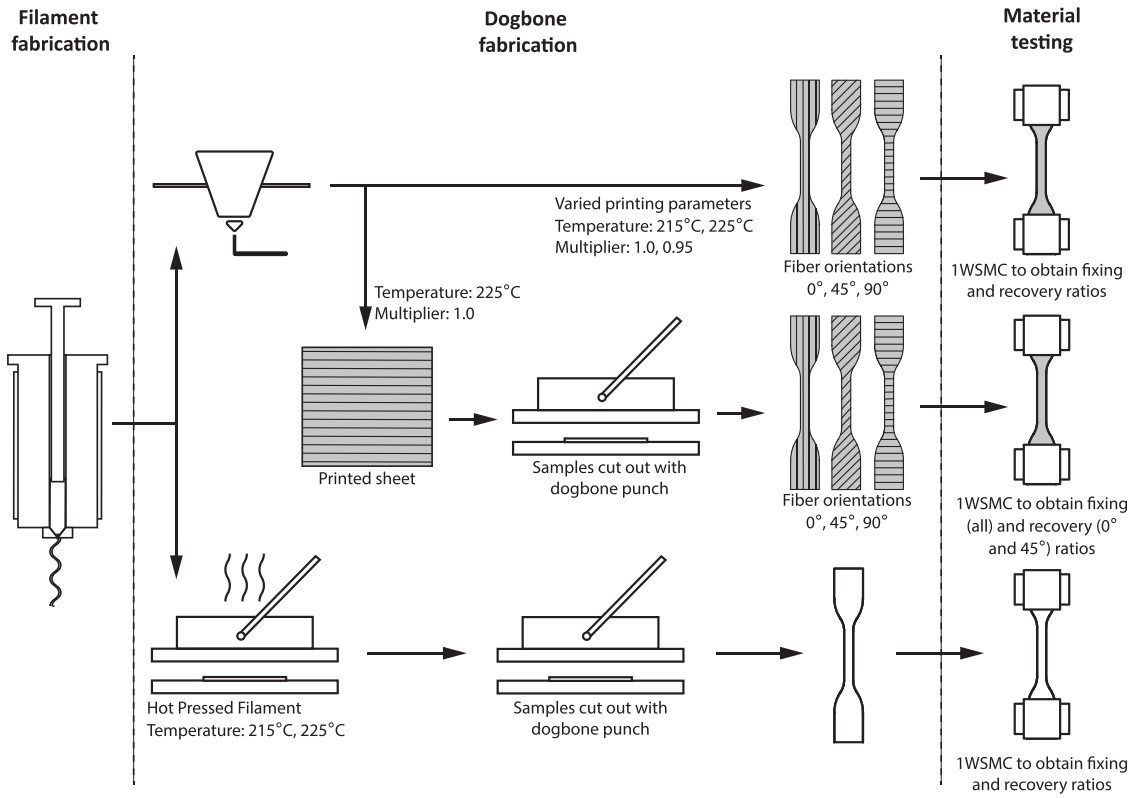

FIG. 1. Study design overview. After fabrication of filament by melt spinning, dogbones are fabricated by printing, by punching from a printed sheet, or by hot pressing. All samples were characterized using a one-way shape-memory cycle analysis. Fixing ratios were calculated for all samples. Recovery ratios were only calculated for 0° and 45° samples due to plastic deformation in 90° samples.

to nozzle translational velocity by controlling the volume of polymer extruded from the nozzle per unit time. An increase or decrease in multiplier will increase or decrease the rotation speed of the feed gears, respectively. Fiber orientation is the direction the material is deposited during printing, with 0° defined in this study as the long axis of the dogbone and 90° corresponding to the width. Preliminary printing was conducted to determine suitable ranges for each parameter. Based on the preliminary printing, the parameters chosen were as follows: temperatures of 215°C and 225°C; extrusion multiplier of 0.95 and 1.0; and fiber orientations of 0°, 45°, and 90° (Figs. 2A and 3A, B). This yielded a total of 12 sample sets (Table 1).

Hot-pressed samples. To control for fiber orientation and multiplier, we created samples of homogeneous material (i.e., no fibers) by hot-pressing SMP filament into films using a benchtop hydraulic press (Carver 3851-0, USA) at 215°C or

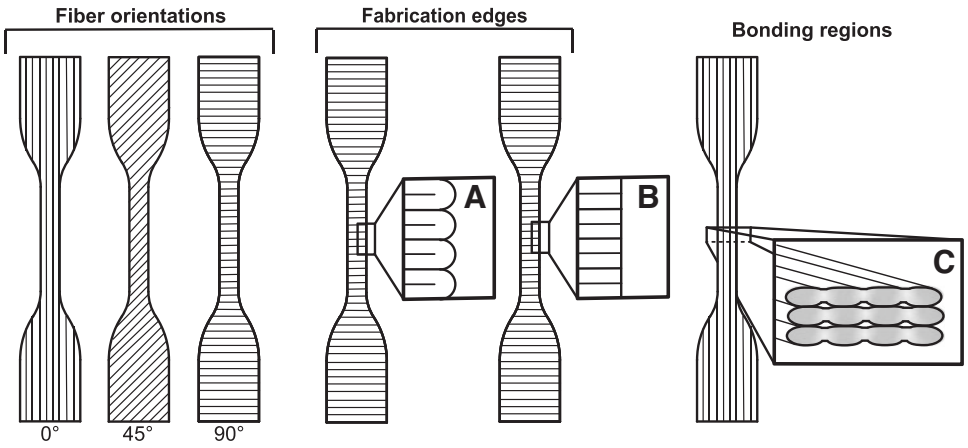

FIG. 2. Raster-printed dogbone schematic showing fiber orientations. *Insets*: **(A)** raster-printed edge showing continuous loops at the edge of the sample, **(B)** punched edge showing no loops, and **(C)** sample cross-section showing the fiber bonding regions. For **(A/B)** and **(C)**, 0° and 90° samples are used for illustrative purposes, but the edge effects and bonding regions shown are relevant to all fiber orientations.

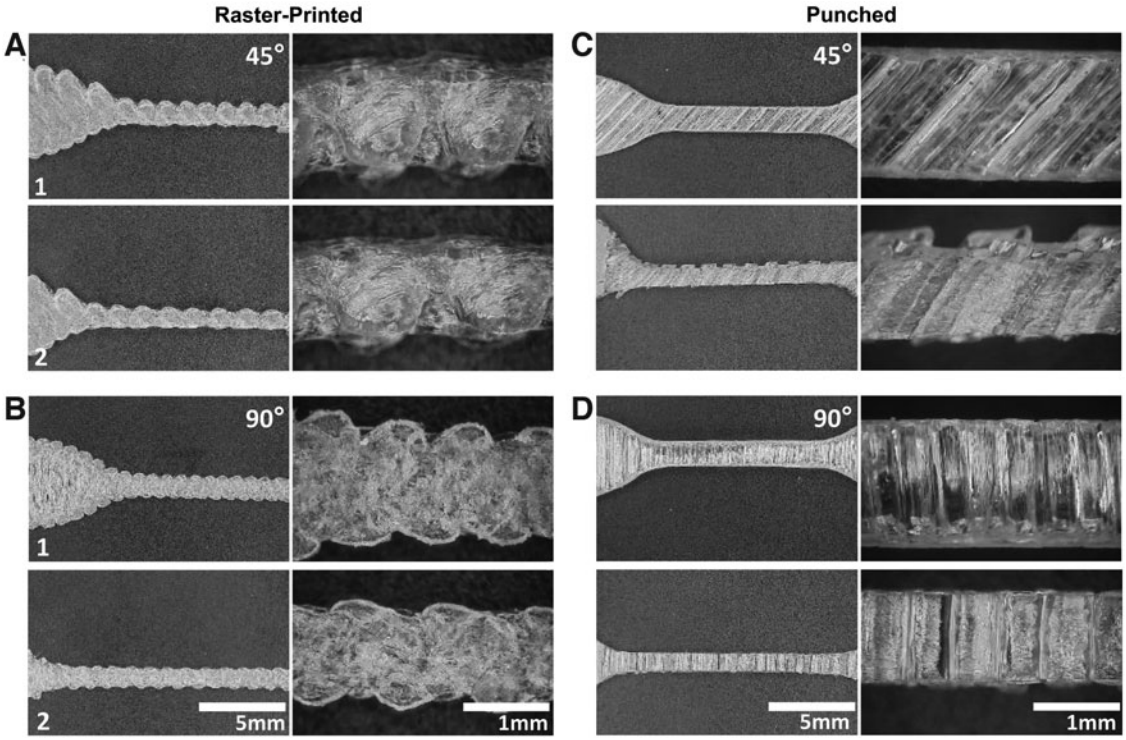

FIG. 3. Images comparing (1) prestretching versus (2) poststretching to show material and fiber fusion behavior of punched and raster-printed samples at 45° **(A, C)** and 90° **(B, D)** orientations.

225°C. Dogbones were punched from the resulting film using a type IV dogbone punch with the same dimensions as the printed dogbones.

Punched samples. To determine if raster print edge effects play a role in fixing or recovery, dogbone samples were also punched from a large printed sheet (Figs. 2B and 3C, D). To fabricate these control samples, a rectangular sheet was printed at 225°C with a multiplier of 1.0 while all other printer settings were kept as described above. From the printed sheet, dogbones were punched out using the same method as the hot-pressed samples. Samples possessing the three different fiber orientations under study were achieved by rotating the punch on the sheet to 0°, 45°, and 90° relative to the fiber direction of the printed sheet.

TABLE 1. RASTER-PRINTED PARAMETERS

Fiber orientation (° to long axis)	*Extrusion rate (multiplier)*	*Print temperature (°C)*
0	0.95	215
		225
	1.0	215
		225
45	0.95	215
		225
	1.0	215
		225
90	0.95	215
		225
	1.0	215
		225

Material characterization

Fixing ratio and recovery ratio. Fixing and recovery ratios were calculated after preforming a 1WSMC using DMA. Samples were loaded into the DMA and, using a force-controlled sequence, heated above T_g to 90°C, isothermally held for 10 min to ensure uniform heating, and then stretched at 0.02 N/min to elongate the samples to 20% of their initial length. Upon reaching 20% strain, the temperature was decreased to 0°C to fix the sample in the strained state. The sample was then heated back to 90°C at 2.0°C/min and held isothermally at 90°C for 10 min to completely recover the sample. This cycle was repeated four times, and the strains from cycles two through four were used to calculate fixing ratio and recovery ratio. For the punched dogbones, which were more sensitive to applied stresses, 0.001 N/min was used during the stretching portion of the cycle to prevent programmed strain from overshooting 20% of their initial length.

Fixing ratio was calculated as

$$R_f(\%) = \frac{\varepsilon_u(N)}{\varepsilon_m(N)} \times 100,$$

and recovery ratio calculated as

$$R_r(\%) = \frac{\varepsilon_u(N) - \varepsilon_p(N)}{\varepsilon_u(N) - \varepsilon_p(N-1)} \times 100,$$

where ε_u is strain after unloading, ε_m is the strain after deformation, and ε_p is the permanent strain after recovery.[36,37] A fixing ratio of 100% indicates that an SMP maintains its

exact temporary shape. A recovery ratio of 100% indicates that an SMP returns to its exact original shape. Ideal shape-memory behavior is considered $R_f = R_r = 100\%$. While the specific application of an SMP tends to determine what constitutes a sufficient fixing ratio or recovery ratio, a ratio $\sim 100\%$ is generally considered favorable and necessary.[37] Fixing and recovery ratios >100% are possible, and indicate expansion of the material during fixing and recovery past the original length, respectively. Both effects can be caused by changes in crystalline alignment during solid-state phase transformation of the polymer chains when heated and cooled.[38]

Cytocompatibility assay

To determine the extent to which printing parameters affect cell viability on the 3D-printed SMP, flat $9.0 \times 9.0 \times 0.4$ mm samples were printed with the same systematically varied temperature and multiplier described above. Fiber orientation was not studied because it is a macroscopic, not microscopic, property and not expected to affect cell behavior. Control samples were cut from tissue culture polystyrene.

C3H10T1/2 murine fibroblasts (ATCC) were seeded onto samples and incubated at 37°C for 48 h. Samples were then stained with LIVE/DEAD (Invitrogen) reagents, per the manufacturer's instructions, and imaged using a Leica DMI 4000B inverted fluorescent microscope. Viability was calculated by dividing the number of live cells by the total number of cells.

Statistical analysis

One-way analysis of variance (ANOVA) was performed with Tukey's honestly significant difference (HSD) test for multiple comparison testing, and a two-way ANOVA was performed for comparisons with multiple variables. Reported p-values are from ANOVA unless otherwise indicated, and p-values between two factors are indicated with a subscript (e.g., "$p_{t,m}$" denotes p-value for interactions between temperature and multiplier, and "$p_{0°,45°}$" denotes p-value of fiber orientation levels comparing 0° and 45°). To determine significant differences in viability of cells on printed substrates, a two-way ANOVA was performed. Means were considered statistically different for $p < 0.05$.

Results

Raster-printed samples

For the raster-printed dogbone samples, fiber orientation had a significant effect on fixing ratio ($p = 4.03 \times 10^{-9}$), but no significant effect was found for temperature ($p = 0.42$), or any interactions ($p_{t,m} = 0.72$, $p_{t,f} = 0.56$, $p_{m,f} = 0.22$). All fiber orientations were statistically different from one another ($p_{0°,45°} = 0.02$, $p_{0°,90°} = 1.0 \times 10^{-6}$, $p_{90°,45°} = 2.0 \times 10^{-6}$, Tukey's HSD; Fig. 4A and Table 2), and a polynomial regression produced relatively high correlation ($R^2 = 0.749$), illustrating the second-order decrease in fixing ratio with increasing fiber orientation. In addition, increasing the degree of fiber orientation from 0° to 45° and to 90° resulted in a significant increase in the distribution of recovery ratio values ($p_{0°,45°} = 6.6 \times 10^{-4}$, $p_{0°,90°} = 5.3 \times 10^{-7}$, $p_{90°,45°} = 0.01$, Bartlett's test; Fig. 4B and Table 2), with polynomial regression demonstrating low correlation ($R^2 = 0.1013$) and a much flatter profile than that observed with the fixing ratio.

Hot-pressed samples

Consistent with our findings from the printed samples, temperature had no significant effect on fixing ratio ($p = 0.98$; Fig. 4A and Table 2) or recovery ratio ($p = 0.089$; Fig. 4B and Table 2).

Punched samples

For punched samples, which control for raster-printed edges, fiber orientation had a significant effect on fixing ratio ($p = 0.004$). Fixing ratios for 0° and 90° samples were statistically different from each other, as were those for 0° and 45° ($p_{0°,45°} = 0.005$, $p_{0°,90°} = 0.01$, Tukey's HSD; Fig. 4A and Table 2). Piecewise linear regression demonstrated relatively high correlation ($R^2 = 0.8414$) from 0° and 45°, illustrating the decrease in fixing ratio with increasing fiber orientation, and demonstrated low correlation ($R^2 = 0.1261$) from 45° to 90°, illustrating the lack of significant effect >45°. Note that we only utilize the regression analysis to indicate the trend of the fixing ratio as a function of fiber orientation due to the limited data. More systematic studies will be conducted in our future work. With respect to recovery ratio, fiber orientations of 90° did not recover after programming, therefore recovery ratios could not be reported for those samples (see Discussion section). The variance of recovery ratio values for 0° and 45° samples was significantly different ($p_{0°,45°} = 1.67 \times 10^{-5}$, F-test; Fig. 4B and Table 2).

Printed versus punched

There was a significant interaction between the effects of fiber orientation and fabrication method on fixing ratio ($p = 0.01$; Fig. 4C and Table 2), where orientations of 0° and 90° showed no significant effect from fabrication method, but there was a significant effect at 45° ($p_{\text{punch, r-print}} = 0.004$, Tukey's HSD). When the fiber orientation was 45°, there was a statistical difference between the 0° and 45° orientations that were punched ($p_{0°,45°} = 0.0003$, Tukey's HSD), which does not appear when the samples were raster printed ($p_{0°,45°} = 0.55$, Tukey's HSD). Differences in recovery ratio were not statistically significant for any of the printing parameters.

Cytocompatibility

Multiplier was found to significantly affect viability ($p = 0.0003$). There was no significant difference detected for temperature ($p = 0.46$) or interactions ($p = 0.69$) (Fig. 5). The total cell numbers for all samples were not significantly different ($p > 0.05$). The cell viability of all samples was >90%, which suggests reasonable cytocompatibility. The samples printed at 215°C and a multiplier of 1.0 had a mean viability of $93.2\% \pm 0.89\%$ and a total cell count ranging from 107 to 558 cells/sample with a mean total cell count of 270 ± 150 cells/sample field of view. The samples printed at 215°C and a multiplier of 0.95 had a mean viability of $95.6\% \pm 1.24\%$ and a total cell count ranging from 121 to 352 cells/sample field of view with a mean total cell count of 212 ± 121 cells/sample field of view. The samples printed at 225°C and a multiplier of 1.0 had a mean viability of $92.4\% \pm 0.51\%$ and a total cell count ranging from 209 to 314 cells/sample field of view with a mean total cell count of 263 ± 53 cells/sample

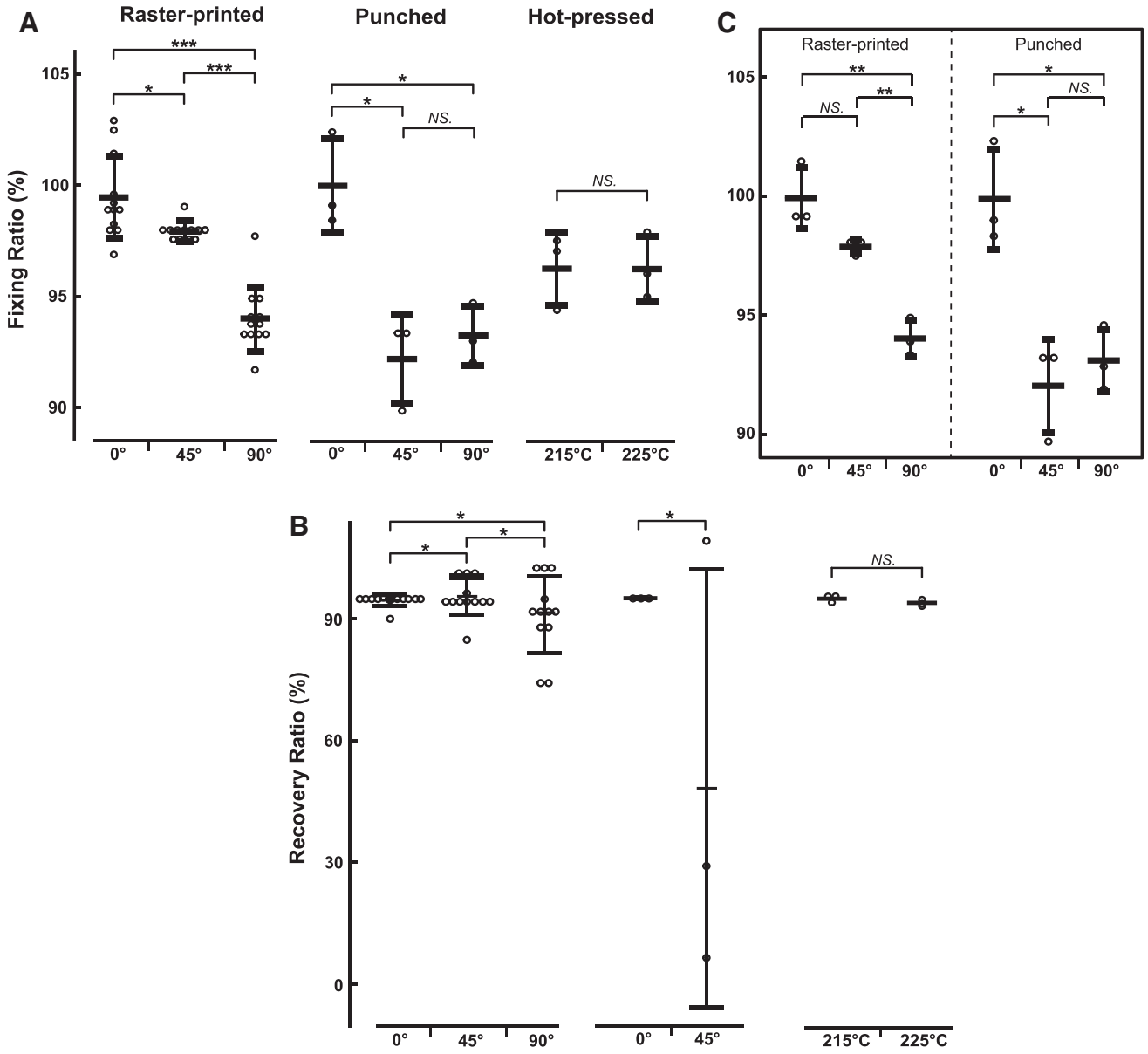

FIG. 4. **(A)** Fiber orientation affects fixing ratio in both raster-printed and punched samples. Crossbars on standard deviations show group means ($*p<0.05$; $***p<0.001$, Tukey's HSD *post hoc*). No significant effects were found for the hot-pressed control groups. **(B)** Fiber orientation significantly affects the variance of recovery ratio of both raster-printed and punched samples. Crossbars on standard deviations show group means ($*p<0.050$ by Bartlett's test for raster-printed samples and F-test for punched samples). No significant effects were found for the hot-pressed control groups. **(C)** For only the subset of samples from **(A)** printed at 225°C with a multiplier of 1.0, interactions between fiber orientation and fabrication method have a significant effect on fixing ratio. Crossbars on standard deviations show group means ($*p<0.05$; $**p<0.005$; NS $p>0.05$, Tukey's HSD *post hoc*). For the polynomial regressions (raster-printed sample fixing and recovery ratios) and piecewise linear regression (punched sample fixing ratio), θ is in units of degrees. HSD, Tukey's honestly significant difference test; NS, no significant difference.

field of view. The samples printed at 225°C and a multiplier of 0.95 had a mean viability of 96.3% ± 0.42% and a total cell count ranging from 151 to 240 cells/sample field of view with a mean total cell count of 203 ± 46 cells/sample field of view.

Discussion

The results showed that printing parameters used in FFF can affect both key shape-memory properties and cytocompatibility of 3D-printed SMPs. In particular,

- fiber orientation significantly impacted both the fixing ratio and the recovery ratio of printed samples and of punched samples;
- multiplier significantly affected cell viability;
- in contrast, temperature and multiplier had little effect on the fixing ratio and recovery ratio; and
- similarly, temperature did not affect cell viability.

In raster-printed samples, the fiber orientation was found to affect mean fixing ratio, but not mean recovery ratio, while

Table 2. Summary of Effects of Printing Parameters on Fixing and Recovery Ratios

Type	*FO*	*Mult*	*Temp*	R_r	R_f
Raster	0	1	215	95.15	100.76
			225	93.58	99.89
		0.95	215	95.86	99.09
			225	95.06	98.07
	45	1	215	97.09	97.72
			225	93.55	97.84
		0.95	215	95.94	97.85
			225	97.18	98.27
	90	1	215	98.02	94.94
			225	91.71	94.01
		0.95	215	86.15	93.58
			225	89.41	93.53
Punched	0	1	225	95.34	99.85
	45	1	225	48.47	92.02
	90	1	225	no recovery	93.09
Hot pressed	n/a	n/a	215	94.64	96.37
	n/a	n/a	225	92.80	96.34

FO, fiber orientation.

temperature and multiplier did not significantly affect either ratio. The data showed that when strain direction was aligned with fiber direction (i.e., the 0° orientation), the average fixing ratio approached 100% (99.45% ± 1.8%). At 45°, fixing ratio was consistently in the upper 90% range with an average of 98%. The 90° orientation had a less consistent fixing ratio and a range of 92–98%. While the mean recovery ratios were not statistically different for each fiber orientation, the data showed a trend of increasing variability in recovery ratio as the orientation increased from 0° to 90°. This suggests that fiber orientation may affect the reliability of the shape-memory behavior of a printed SMP.

Similar trends were found in the punched sample data, which revealed a fiber orientation effect on fixing ratio. Unlike the raster-printed samples, there was no significant difference between 45° and 90° fiber orientation for fixing. Also, punched samples at 90° orientations did not recover once programmed during the 1WSMC. This suggests that the edge behavior of the raster print path contributes to the overall behavior of the shape-memory sample. Additional support for this speculation was seen in the comparisons between the punched and the raster-printed samples that were fabricated at 225°C and a multiplier of 1 (Fig. 4C). Considering fixing ratio, when printed the 45° orientation had shape-memory behavior similar to the printed 0° orientation, but when punched had shape-memory behavior similar to that of the punched 90° orientation.

Fiber orientation also affected the distribution of recovery ratios for both the raster-printed and punched samples. For example, in the raster-printed dogbones, 0° samples had recovery ratios that ranged from 90% to 98%, 45° samples ranged from 85% to 102%, and 90° samples ranged from <80% to 104%. The standard deviation of each recovery ratio was significantly different than all others. The same trend is seen in the samples that were punched, where the 0° orientations had values tightly clustered ~95%, while the 45° orientation had a range from <10% to 109%. These findings suggest that fiber orientation can affect the distribution of recovery ratio values and contribute to less reliable shape-memory behavior when the fiber orientation is not aligned with the loading direction.

A possible explanation for the trend in fiber orientation is mechanical deformation of the fusion regions between fibers. Bellehumeur *et al.* described these fusions as sintering or semimolten coalescence of printed fibers.[39] They found that the strength of the bonding is highly dependent on printing temperature, and that higher temperatures led to stronger bonding and greater contact area. However, they found that the fibers cool too rapidly to ensure complete bonding, and therefore the properties of the bonding region are different from those of the fibers. In this study, as fiber orientation increased to 90°, fibers became less aligned with the loading direction as applied during shape-memory programming in the DMA. Therefore, at the higher angles, the loading

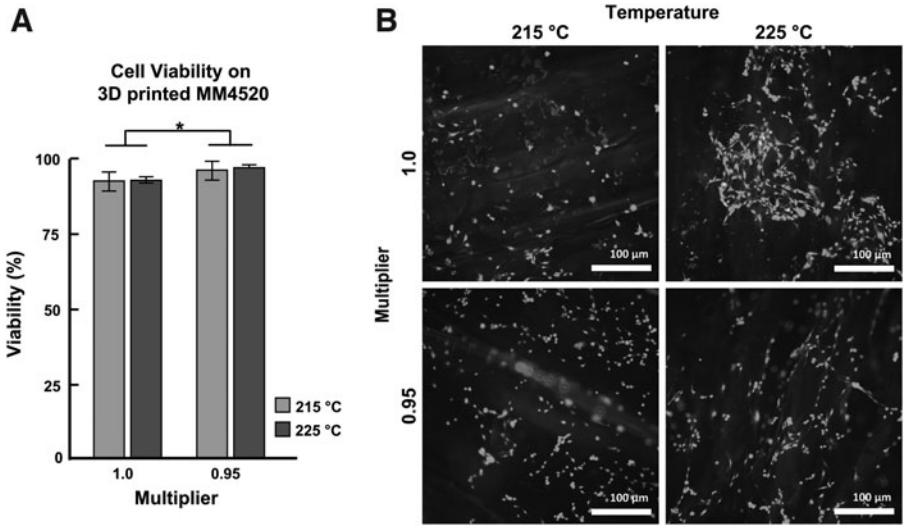

FIG. 5. **(A)** Extrusion multiplier has a significant effect on cell viability. No significant difference in viability due to temperature was detected. Crossbars on standard deviations show group means (*$p < 0.05$; two-way ANOVA). **(B)** Representative images of cell viability on samples printed with varied combinations of temperature and extrusion multiplier. ANOVA, analysis of variance.

increasingly occurred not only in the fiber but also in the width of the fusion points between fibers. If mechanical properties are weaker in the fusion region compared with the width of the fibers due to incomplete bonding and a smaller cross-sectional area[39,40] (Fig. 2C), the effects of fiber orientation observed in our study could be explained by plastic deformation in the bonding regions. As fiber orientation increases to 90°, plastic deformation in the bonding regions would affect the ability of the sample to remain fixed and to recover, due to local material damage, including chain disentanglement[36] and microcracks.[41] The extra material that is laid down in a raster-printed edge could stabilize the 45° and 90° samples because the additional loop of material stretches in the direction of strain and reduces the concentration of stress in the bonding regions. This would lessen the severity of the plastic deformation of the material in the bonding regions, which would allow better fixing and recovery of the SMP. The raster-edge stabilization effect would be anticipated to diminish with increasing size of the printed object. For example, had our study used a larger dogbone, the size of the loops relative to the dimensions of the sample cross-section would be smaller, which would diminish the edge effects.

Temperature and multiplier are among the most common user-adjusted print settings, and to produce high-fidelity SMP parts through 4D printing, it is critical to understand how even a small change in setting might impact shape-memory behavior. Regarding temperature, polymers can be printed within a range of temperatures, and our preliminary studies revealed that the SMP used in this work can be printed as low as 210°C and as high as 230°C. As printing temperatures approach the low end of the range, the molten polymer becomes increasingly viscous and leads to nozzle clogging. At the high end of the range, bubbles form in the extruded fiber and the material also shows signs (discoloration) of degradation. Temperatures of 215°C and 225°C were chosen for the present work, because both are well within the printing range and have enough separation to prevent any over- or undershooting (a consequence from the sensitivity of the printer's temperature sensor) of the temperature, overlapping, or deviation outside of the target range. The small temperature range for this particular SMP rendered study of additional temperatures unnecessary.

Regarding the extrusion multiplier parameter, the multiplier has been shown to influence the porosity of 3D-printed objects and is commonly adjusted for part quality purposes. In most FFF 3D printers, including the MakerBot used in this work, the flow rate is automatically calibrated by the printing software to ensure adequate material extrusion for the travel speed specified by the user.[42] For our SMP we used 1.0 (printer default), and 0.95, which is equivalent to 95% of the calculated gear rotation speed.

We also confirmed the cytocompatibility of the SMP when 3D printed using different printing temperatures and multipliers. Cell viability for all printed samples was >90%, representative of a high degree of viability, which supports the cytocompatibility reported previously.[16] A reduced multiplier contributed to a higher cell viability, which could potentially be explained by the resulting reduction in fiber diameter that could produce small spaces between the fibers and create a suitable microenvironment providing proximity to other cells, minimal stress, increased adhesion, and maintenance of temperature and nutrients.[43,44]

The 4D printing field is growing rapidly, and investigations of 4D-printed SMPs beyond the fundamental considerations in this work include studies to evaluate printing parameters' effect on prestrain in the printed SMP.[35,45] The prestrain is used as a programming mechanism for the SMP during printing, and has the potential to create self-morphing objects and parts. Before such advancement can be regularly implemented in the field, there must be a robust understanding of how the parameters impact the shape-memory behavior of printed objects. Here, we have provided insight into the effects of printing parameters using commercially available SMP and FFF technology, and our findings suggest that other available 4D printing technology should be similarly evaluated.

Conclusion

This study demonstrated the impact of printing parameters on the shape-memory behavior and cell viability of 3D-printed SMPs. We found that fiber orientation has the most significant effect on shape-memory properties, where an increase in fiber orientation from 0° to 90° decreases the fixing ratio and increases the variance in recovery ratios, likely due to local plastic deformations of the bonding regions between fibers. We also found that multiplier has a significant effect on cell viability, but that all printing parameters studied showed high cytocompatibility. These findings indicate that it is essential to carefully plan the print path of a 3D-printed SMP part, so that the fibers orient optimally with the direction of programmed strain for the prescribed application. Failure to do so could result in poor fixing and recovery, resulting in an SMP device with a questionable ability to perform its intended function.

Acknowledgments

The authors gratefully acknowledge the efforts of Paul Chando, for his expertise in 3D printing technology, and James Pieri, for his assistance with CAD.

Author Disclosure Statement

No competing financial interests exist.

Funding Information

Financial support for this project was provided by the National Science Foundation Biomaterials and Advanced Manufacturing programs (DMR-1609523 and CMMI-2022421), the Syracuse University Collaboration of Unprecedented Success and Excellence (CUSE) program, and the Syracuse University Research Excellence Doctoral Funding program.

Supplementary Material

Supplementary Data

References

1. Wang J, Quach A, Brasch ME, *et al.* On-command on/off switching of progenitor cell and cancer cell polarized motility and aligned morphology via a cytocompatible shape memory polymer scaffold. Biomaterials 2017;140:150–161.

2. Brasch ME, Id GP, Gulvady AC, *et al.* Nuclear position relative to the Golgi body and nuclear orientation are differentially responsive indicators of cell polarized motility. PLoS One 2019;1–19.
3. Passucci G, Brasch ME, Henderson JH, *et al.* Identifying the mechanism for superdiffusivity in mouse fibroblast motility. PLoS Comput Biol 2019;15:1–16.
4. Gong T, Zhao K, Yang G, *et al.* The control of mesenchymal stem cell differentiation using dynamically tunable surface microgrooves. Adv Healthc Mater 2014;3:1608–1619.
5. Luo R, Wu J, Dinh ND, *et al.* Gradient porous elastic hydrogels with shape-memory property and anisotropic responses for programmable locomotion. Adv Funct Mater 2015;25:7272–7279.
6. Gu H, Lee SW, Buffington SL, *et al.* On-demand removal of bacterial biofilms via shape memory activation. ACS Appl Mater Interfaces 2016;8:21140–21144.
7. Wang J, Brasch ME, Baker RM, *et al.* Shape memory activation can affect cell seeding of shape memory polymer scaffolds designed for tissue engineering and regenerative medicine. J Mater Sci Mater Med 2017;28:1–9.
8. Zimkowski MM, Rentschler ME, Schoen J, *et al.* Integrating a novel shape memory polymer into surgical meshes decreases placement time in laparoscopic surgery: An in vitro and acute in vivo study. J Biomed Mater Res A 2013;101:2613–2620.
9. Zarek M, Mansour N, Shapira S, *et al.* 4D printing of shape memory-based personalized endoluminal medical devices. Macromol Rapid Commun 2017;38:1–6.
10. Ligon SC, Liska R, Stampfl J, *et al.* Polymers for 3D printing and customized additive manufacturing. Chem Rev 2017;117:10212–10290.
11. Ge Q, Sakhaei AH, Lee H, *et al.* Multimaterial 4D printing with tailorable shape memory polymers. Sci Rep 2016;6:1–12.
12. Ding Z, Yuan C, Peng X, *et al.* Direct 4D printing via active composite materials. Sci Adv 2017;3:e1602890.
13. Lendlein A, Langer R. Biodegradable, elastic shape-memory polymers for potential biomedical applications. Science 2002;296:1673–1676.
14. Jia H, Gu SY, Chang K. 3D printed self-expandable vascular stents from biodegradable shape memory polymer. Adv Polym Technol 2018;37:3222–3228.
15. Rychter P, Pamula E, Orchel A, *et al.* Scaffolds with shape memory behavior for the treatment of large bone defects. J Biomed Mater Res A 2015;103:3503–3515.
16. Farè S, Valtulina V, Petrini P, *et al.* In vitro interaction of human fibroblasts and platelets with a shape-memory polyurethane. J Biomed Mater Res - Part A 2005;73:1–11.
17. De Nardo L, Alberti R, Cigada A, *et al.* Shape memory polymer foams for cerebral aneurysm reparation: Effects of plasma sterilization on physical properties and cytocompatibility. Acta Biomater 2009;5:1508–1518.
18. Metcalfe A, Desfaits AC, Salazkin I, *et al.* Cold hibernated elastic memory foams for endovascular interventions. Biomaterials 2003;24:491–497.
19. Rastogi P, Kandasubramanian B. Breakthrough in the printing tactics for stimuli-responsive materials: 4D printing. Chem Eng J 2019;366:264–304.
20. Tibbits S. 4D printing: Multi-material shape change. Archit Des 2014;84:116–121.
21. Momeni F, M.Mehdi Hassani.N S, Liu X, *et al.* A review of 4D printing. Mater Des 2017;122:42–79.
22. Choi J, Kwon O-C, Jo W, *et al.* 4D printing technology: A review. 3D Print Addit Manuf 2015;2:159–167.
23. Baker RM, Henderson JH, Mather PT. Shape memory poly(ε-caprolactone)-co-poly(ethylene glycol) foams with body temperature triggering and two-way actuation. J Mater Chem B 2013;1:4916–4920.
24. Koerner H, Price G, Pearce NA, *et al.* Remotely actuated polymer nanocomposites—Stress-recovery of carbon-nanotube-filled thermoplastic elastomers. Nat Mater 2004;3:115.
25. Sahoo NG, Jung YC, Cho JW. Electroactive shape memory effect of polyurethane composites filled with carbon nanotubes and conducting polymer. Mater Manuf Process 2007;22:419–423.
26. Buffington SL, Paul JE, Ali MM, *et al.* Enzymatically triggered shape memory polymers. Acta Biomater 2019;84:88–97.
27. Alsop T. ''Most used 3D printing technologies 2020.'' *Statista* (2020).
28. Davis KA, Luo X, Mather PT, *et al.* Shape memory polymers for active cell culture. J Vis Exp 2011;2–6.
29. Tseng LF, Mather PT, Henderson JH. Shape-memory-actuated change in scaffold fiber alignment directs stem cell morphology. Acta Biomater 2013;9:8790–8801.
30. Baker RM, Tseng L-F, Iannolo MT, *et al.* Self-deploying shape memory polymer scaffolds for grafting and stabilizing complex bone defects: A mouse femoral segmental defect study. Biomaterials 2016;76:388–398.
31. Villacres J, Nobes D, Ayranci C. Additive manufacturing of shape memory polymers: Effects of print orientation and infill percentage on mechanical properties. Rapid Prototyping J 2018;24:744–751.
32. Yang Y, Chen Y, Wei Y, *et al.* 3D printing of shape memory polymer for functional part fabrication. Int J Adv Manuf Technol 2016;84:2079–2095.
33. Garcia Rosales CA, Kim H, Garcia Duarte MF, *et al.* Characterization of shape memory polymer parts fabricated using material extrusion 3D printing technique. Rapid Prototyping J 2019;25:322–331.
34. Abuzaid W, Alkhader M, Omari M. Experimental analysis of heterogeneous shape recovery in 4D printed honeycomb structures. Polym Test 2018;68:100–109.
35. Bodaghi M, Damanpack AR, Liao WH. Adaptive metamaterials by functionally graded 4D printing. Mater Des 2017;135:26–36.
36. Rousseau IA. Challenges of shape memory polymers: A review of the progress toward overcoming SMP' s limitations. Epub ahead of print 2008. DOI: 10.1002/pen.
37. Mather PT, Luo X, Rousseau IA. Shape memory polymer research. Annu Rev Mater Res 2009;39:445–471.
38. Jang BZ, Zhang ZJ. Thermally- and phase transformation-induced volume changes of polymers for actuator applications. J Intell Mater Syst Struct 1994;5:758–763.
39. Bellehumeur C, Li L, Qian S, *et al.* Modeling of bond formation between polymer filaments in the fused deposition modeling process. J Manuf Processes 2004;6:170–178.
40. Li, L. (2002). Analysis and fabrication of FDM prototypes with locally controlled properties (Unpublished doctoral thesis). University of Calgary, Calgary, AB. DOI:10.11575/PRISM/21634.

41. Shojaei A, Li G, Voyiadjis GZ. Cyclic viscoplastic-viscodamage analysis of shape memory polymers fibers with application to self-healing smart materials. J Appl Mech Trans ASME 2013;80:1–15.
42. Gordeev EG, Galushko AS, Ananikov VP. Improvement of quality of 3D printed objects by elimination of microscopic structural defects in fused deposition modeling. *PloS one* 13.6 2018:e0198370.
43. Walker GM, Zeringue HC, Beebe DJ. Microenvironment design considerations for cellular scale studies. Lab Chip 2004;4:91–97.
44. Huang G, Li F, Zhao X, *et al.* Functional and biomimetic materials for engineering of the three-dimensional cell microenvironment. Chem Rev 2017;117:12764–12850.
45. Hu GF, Damanpack AR, Bodaghi M, *et al.* Increasing dimension of structures by 4D printing shape memory polymers via fused deposition modeling. Smart Mater Struct 2017;26. DOI: 10.1088/1361-665X/aa95ec

Address correspondence to:
James H. Henderson
Department of Biomedical and Chemical Engineering
BioInspired Syracuse
318 Bowne Hall
Syracuse, NY 13244
USA

E-mail: jhhender@syr.edu